Available online at www.sciencedirect.com
ScienceDirect
Journal of Solid State Chemistry 180 (2007) 765–771
JOURNAL OF SOLID STATE CHEMISTRY
www.elsevier.com/locate/jssc

# Charge transport properties in microcrystalline $KDyFe(CN)_6$

P.H. Aubert, F. Goubard*, C. Chevrot, A. Tabuteau

*Laboratoire de Physico-Chimie des Polymères et des Interfaces (LPPI), Université de Cergy-Pontoise, 5 Mail Gay-Lussac, Neuville-sur-Oise 95031, Cergy-Pontoise Cedex, France*

Received 29 June 2006; received in revised form 30 November 2006; accepted 3 December 2006
Available online 8 December 2006

**Abstract**

Microcrystalline solid dysprosium(III) hexacyanoferrate(II) was synthesized by co-precipitation in aqueous solution. The resulting solid has been studied by Fourier transform infrared spectroscopy, X-ray analysis and solid state electrochemistry. The use of a cavity microelectrode was necessary to explore a wide range of time scale and minimize the (undesired) capacitive currents. Cyclic voltametric experiments were very helpful to understand the kinetic of charge transfer in such microstructure. A structure–properties relationship has been established from the crystallographic and the electrochemical properties. A square-scheme is presented to explain the unique electrochemical behavior of hexacyanoferrate containing dysprosium since this compound exhibits a second redox system. The solid presents an open channel-like morphology in which the motion of charged species occurs during the redox processes. Precisely, the electronic transfer is accompanied by a cation diffusion inside the microcrystalline structure. The size of these channels strongly suggests that the kinetic of charge transfer is limited by the cation transport into these structures.


*Keywords:* Dysprosium hexacyanoferrate; Microcrystalline structure; Charge transport; Cavity microelectrode

## 1. Introduction

Prussian blue and related metal hexacyanoferrates [1,2] belong to the class of polymeric inorganic compounds that have been studied extensively for many years. Additional redox chemistry studies associated with these compounds are available [2–11]. Several interesting properties were studied such as ion-exchange [12], electrochromic [2,13], mixed-valence electrical conductivity [14,15], charges (electron, countercation) storage capabilities and related ionic conductivity through zeolitic-like pores [2,7,14–16]. The electrochemical reactions of the metal hexacyanoferrate ions are accompanied by an ion flux (usually an alkali metal cation) from the solid compound to the adjacent solution for charge compensation. The electrochemical response of metal hexacyanoferrates is strongly dependent on the degree of order of the structure, and the nature of counterions which are necessary to maintain the electroneutrality when the electrochemical processes occur.

To understand the problems related to the insertion and lattice accommodation of counterions of various sizes, we have synthesized microcrystalline potassium lanthanide hexacyanoferrates ($Ln$ = Ce–Lu). From a structural point of view, these materials are attractive due to the possible systematic study in relation with the electrochemical responses. The lanthanide ion size involves an important structural deformation from the Prussian Blue structure: $KLnFe(CN)_6 \cdot 4H_2O$ ($Ln$ = La–Nd) [17–20] and $KLnFe(CN)_6 \cdot 3.5H_2O$ ($Ln$ = Gd–Lu) [21–23] crystallize, respectively, in the hexagonal space group $P63/m$ and in the orthorhombic space group $Cmcm$. Otherwise this flexibility is demonstrated by the existence of $Na^+$ to $Cs^+$ in alkali ion site without major structural deformation [24]. To our knowledge, only few papers were dedicated to the electrochemical study of lanthanide metal hexacyanoferrates, the reason being related to their insolubility. A way out consists in synthesizing the compound electrochemically, by modifying a glassy carbon electrode surface. This was achieved by Liu and Chen [25]: they synthesized electrochemically a lanthanum hexacyanoferrate derivative on Pt electrode and characterized the effect of proton on

*Corresponding author. Fax: +33 1 34 25 70 71.
*E-mail address:* fabrice.goubard@u-cergy.fr (F. Goubard).

0022-4596/$ - see front matter © 2006 Elsevier Inc. All rights reserved.
doi:10.1016/j.jssc.2006.12.004

the electrochemical properties. In a similar manner, Cai et al. [26–28] published several papers on the synthesis of samarium and dysprosium hexacyanoferrates modified electrodes with an extensive overview of their transport properties. For insoluble powder materials, the use of composite electrodes is generally necessary: in this case, the powder is mixed with graphite or carbon black as a pellet [29] with some additional binders that help to improve the mechanical properties [30]. To investigate the electrochemical properties of an insoluble material, Sholtz et al. [11,31] have developed a new type of electrodes namely "particle impregnated graphite electrode" in which the powders are mechanically attached to the carbon electrode impregnated with some paraffin. Another technique was developed by Yu et al. [32–34]: they produce a microcavity generated at the Pt surface of a microelectrode, so-called "cavity microelectrode" (CME) in which the insoluble materials are confined close to the electrode surface. The main advantage of this technique is the possibility to study the charge transport properties in wide time scale. That's the reason we choose the CME in the present study.

Here, we report the results concerning the structure of dysprosium hexacyanoferrate, and its electrochemical behavior. Solid state electrochemistry proved to be very powerful as an analytical technique for the study of metal hexacyanoferrates. The CME allows for considerably decreasing the capacitive currents given that quantity of electroactive matter is in the sub-microgram range and the electrochemical interface area is of a fraction of a millimeter square. The CME technique is particularly interesting in the present study, since the electrochemical kinetics of processes occurring at powder material electrode can be easily studied with respect to transport of ions within the microcrystalline solid.

## 2. Experimental

All the chemicals were of p.a. quality and supplied from Acros. All the solutions were prepared using ultrapure water. The iron dysprosium cyanides $KDyFe(CN)_6 \cdot 3.5H_2O$ was synthesized by mixing aqueous solutions of $K_4Fe(CN)_6 \cdot 4H_2O$ ($10^{-2}$ M) and $Dy(NO_3)_3 \cdot 6H_2O$ ($10^{-2}$ M). The fine and microcrystalline powder were filtered off, washed and dried in air.

The X-ray powder diffraction (XRD) analysis was carried out using a Enraf–Nonius diffractometer with Cu$K\alpha$ radiation. The infrared spectra were recorded on a Bruker-Equinoxe FTIR spectrophotometer (the samples were dispersed and pressedinto KBr pellets) over the frequency range 400–4000 $cm^{-1}$. The electrochemical measurements were performed on an Autolab100 potentiostat/galvanostat controlled via computer using GPES electrochemical software. The electrochemical experiments were carried out with a two-compartments glass cell using a three-electrodes system. The reference electrode was a saturated KCl calomel electrode, and a platinum wire was used as the counter-electrode. The working electrode was the CME. Schematically, this CME is made of a glass tube (5–6 mm diameter with a total length ranging from 80 to 150 mm) embedding a Pt-wire (diameter of wire: 50 μm). The cavity was obtained by controlling the dissolution of the platinum in a highly concentrated and warm solution of $HCl + HNO_3$ for 5–30 min. The deepness of the microcavity was measured with a microscope equipped with a digital camera unit fitted to a computer for image processing. The usual height/diameter ratio was between 0.4 and 1. The cavity was filled up with $KDyFe(CN)_6 \cdot 3.5H_2O$ powder using the electrode as a pestle. The filling of the cavity was controlled with microscope, and it was verified that no grains remains on the head outside the cavity. In order to study the influence of the chemical nature of the supporting electrolyte on the electrochemical behavior the dysprosium hexacyanoferrate powder, continuous cycling between 0.0 and 1.0 V was carried out until a stable cyclic voltammogram (CV) was obtained. After the electrochemical experiment, the electroactive powder was eliminated by immersing the cavity electrode in $H_2O_2$ aqueous solution under ultrasonic treatment for 30 min.

## 3. Results and discussion

The FTIR spectrum of dysprosium hexacyanoferrate (Fig. 1A) leads to the following information: a strong and broadband absorption due to C≡N stretching vibrations is observed (2077 $cm^{-1}$). The bands at 470 and 600 $cm^{-1}$ are assigned to the stretching mode of Fe–C (of $FeC_6$ octahedron) and the bending mode of Fe–C≡N, respectively.

A strong absorption band between 3200 and 3400 $cm^{-1}$ corresponds to uncoordinated water.

For $KLnFe(CN)_6 \cdot 4H_2O$ ($Ln$ = La–Nd) in which three water molecules are coordinated to $Ln$ atom, one medium sharp band near 3600 $cm^{-1}$ characteristic of OH stretching and two medium bands (1600–1620 $cm^{-1}$) characteristic of the H–O–H bending appear. In this structure, oxygen atoms are partially coordinated to the lanthanide atom, the symmetry is lowered and new types of absorption bands are observed: e.g., splitting of the 3600 $cm^{-1}$ peak corresponding to the OH stretching frequency is in agreement with structural results.

XRD pattern of the dysprosium hexacyanoferrate is shown in Fig. 1B. All the peaks in the powder X-ray diffraction pattern can be indexed in an orthorhombic $Cmcm$ space group with unit-cell volume $V$ equal to 615.0(2) $Å^3$, where $a = 7.271(1)$ Å, $b = 12.460(2)$ Å, and $c = 13.590(2)$ Å in agreement with ionic radii values. The morphology studied by TEM, was found to be the same as previous work [22], i.e., spherical particles with 1 μm size. The crystal structure of $KDyFe(CN)_6 \cdot 3.5H_2O$ [23] is a three-dimensional (3D) network of corner-sharing $FeC_6$ and $DyN_6O_{2.5}$ units as shown in Fig. 2. Each carbon of $FeC_6$ octahedron is bounded to a surrounding nitrogen of $DyN_6O_{2.5}$ groups. The dysprosium ion is bonded to six

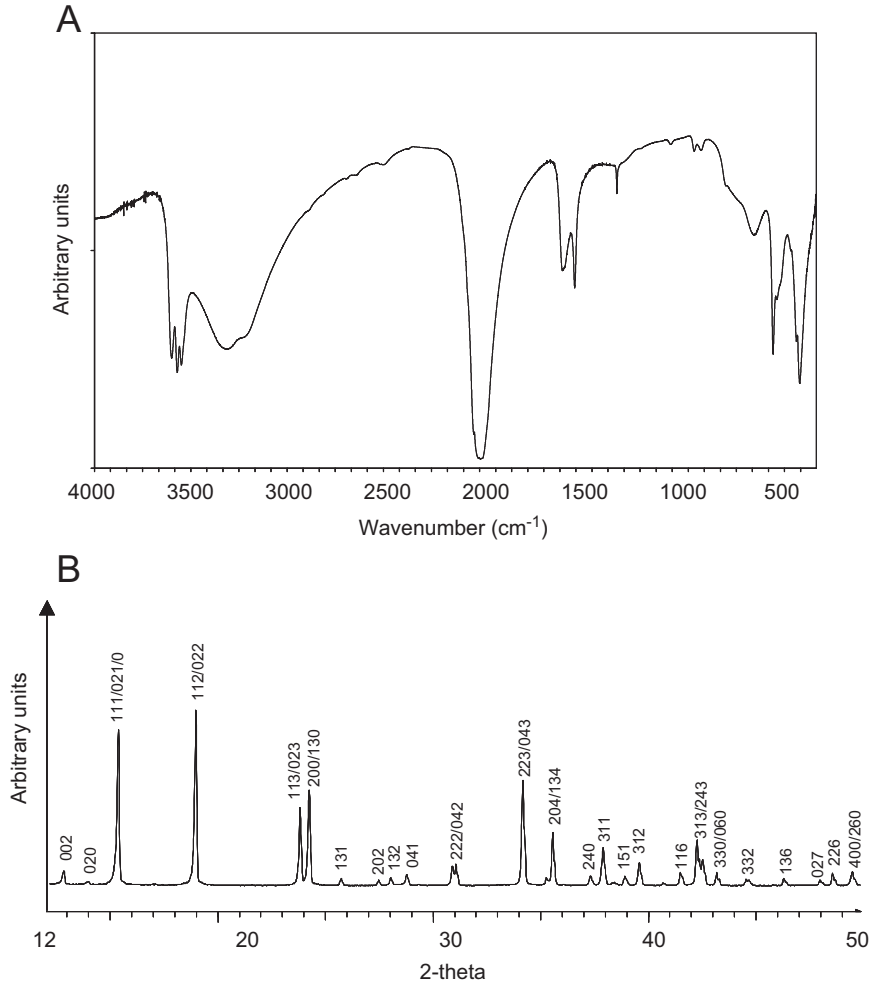


Fig. 1. (A) Infrared spectrum and (B) powder X-ray diffraction pattern for $KDyFe(CN)_6 \cdot 3.5H_2O$.

nitrogen atoms in apical positions (three above and three below the central ion) and to 2.5 water molecules. The Dy groups are linked by non-linear cyanide bridges Dy–N–C–Fe to the octahedral $FeC_6$. The non-linear bridging brings a kind of undulation which produces cavities throughout the structure. These cavities lead to well-defined channels in which the occluded water molecules and potassium ions are located. This latter are located above and below each trigonal prism. They forms a pseudo-hexagonal 2D sublattice near $z = 0$ and 1/2 levels (Fig. 3, top). They are connected to each other by tunnels.

The site of $K^+$ is surrounded by three nitrogen and three oxygen atoms in an antiprism and six nitrogen atoms in equatorial positions (Fig. 3, bottom), the site coinciding with the Wyckoff position 8*f* in *Cmcm*. Two kinds of faces can be distinguished: (i) the top and bottom faces which are isoceles triangles and (ii) the lateral faces up and down the equatorial plane.

To gain a better understanding on the redox processes that can occur within the solid upon electronic transfer, electrochemical measurements have been carried out by means of a CME. Fig. 4 shows the typical CV of microcrystalline solid $KDyFe(CN)_6$ in 1 M KCl solution in a wide range of scan rates (25, 50, 100, 200, 400, 800, 1200 and 1600 mV/s). Since the reduction of dysprosium (III) requires highly negative potentials, the formal potential $E^{\circ\prime} = 0.50$ V (vs. ECS) evaluated at 25 mV/s from the average of the oxidation and reduction process is unambiguously due to the redox couple of the iron centers in the potential range from 0.0 to 1.0 V. This value is higher than that of literature ($E^{\circ\prime} = 0.425$ V, see Ref. [28]) and can be explained by our electrochemical system in which the ohmic drop compensation is a crucial step in order to correct the CVs shape. The experimental data, such as peak current and peak potentials vs. the scan rate $v$ are summarized in Table 1. The electrochemical process can be proposed as the following equation:

$$KDy[Fe^{II}(CN)_6] \rightleftharpoons Dy[Fe^{III}(CN)_6] + K^+ + e^-. \quad (1)$$

As in the case of the iron hexacyanoferrate (Prussian blue), a mixed conduction mechanism (electronic and ionic) occurs during the potentiodynamic perturbation subjected to the modified electrode. For a mixed conduction mechanism, the cation diffusion and the electron

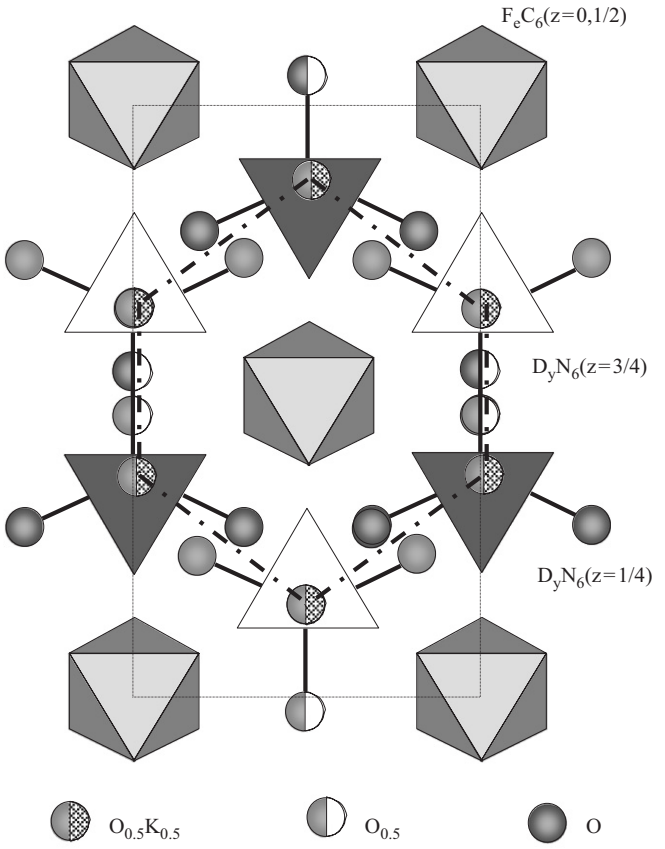


Fig. 2. Schematic representation of the *Ln* and Fe polyhedra packing in the cell of $KDyFe(CN)_6 \cdot 3.5H_2O$. Occluded water molecules and potassium ions form a pseudohexagonal 2D sub-lattice (broken line) connected to each other by tunnels.

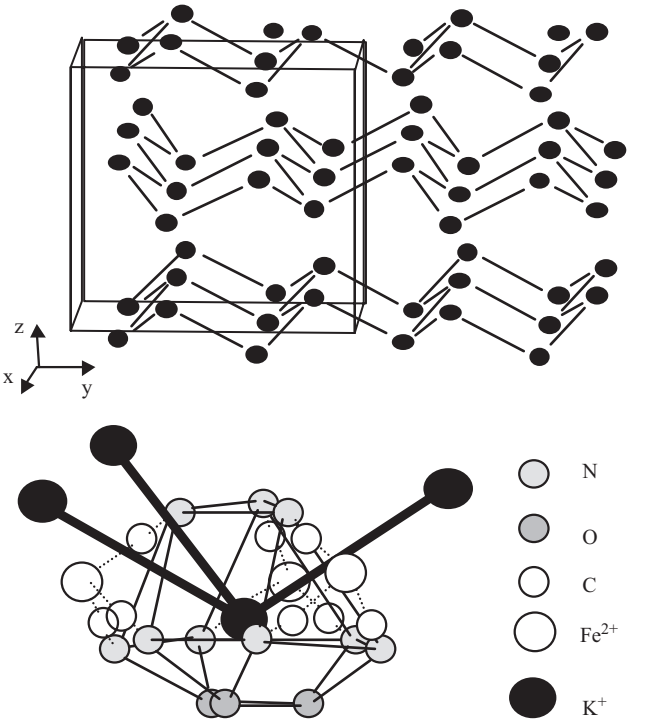


Fig. 3. Top: schematic representation of the conduction channels (thick lines) in the $KDyFe(CN)_6 \cdot 3.5H_2O$ structure. The site for $K^+$ is represented by closed circles. Bottom : environment of the $K^+$.

transfer are interdependent; such process is necessary to maintain the electroneutrality. In order to determine the rate limiting step (the electron transfer or the ionic transfer process), the influence of the time scale has been performed by modifying the scan rate. The increase of the peak separation vs. the scan rate is displayed in Fig. 5A in the range 25–1600 $mV\,s^{-1}$. Such a behavior is typical of a quasi-reversible system and may be indicative for the implication of an E–C mechanism (where (E) is the electrochemical process and (C) a chemical step) during which the slow transfer of cations between the $KDyFe(CN)_6$ and the solution would be the chemical and limiting step of the mechanism. The inset of Fig. 4 displays the ratio between the anodic and cathodic peak currents vs. the logarithm of the scan rate. At low scan rates, this ratio is constant. However, upon decreasing the time scale (high scan rates), this ratio decreases. Such information is also helpful to validate the hypothesis of a chemical step following an electrochemical one.

The variation of the peak current as a function of the scan rate (time scale) allows us to study the mechanisms of the redox processes. According to the Laviron's theory [35–37], the peak current $i_p$ obeys a power-law dependence with respect to the scan rate $v$ ($V\,s^{-1}$):

$$i_p \propto v^{\beta}. \tag{2}$$

If $\beta = 1$, the system has a thin-layer behavior where the diffusion is not implied in the rate limiting step, and the charge consumed during redox processes does not depend upon the time scale. On the other hand, when an ideal planar diffusion process controls the electrochemical response, then $\beta = 1/2$. The Fick's law explains such dependence [37,38]. The value of $\beta$ can be determined from the slope of the logarithm plot of the current as a function of the scan rate. Fig. 5B shows a good linear fit with a $\beta$ slope of 0.532 ($r = 0.997$) or 0.488 ($r = 0.994$) for the anodic or cathodic redox process, respectively. For $KDyFe(CN)_6$ in cavity microelectrode, the experimental values of $\beta$ are close to 0.5, which is consistent with a diffusion process of $K^+$ into the microcrystalline structure. Therefore, the evolution of the charge vs. the time scale should decrease upon time scale. The scan rate dependency of anodic charge presented in Fig. 6 indicates such a trend. Assuming that all electroactive $KDyFe(CN)_6$ in the cavity microelectrode are oxidized even at higher scan rates, we consider that the most likely limiting step in the redox process is the diffusion of counter-cations inside the microcrystalline structure. The previous Eq. (1) is modified according to a E–C mechanism, where the chemical step

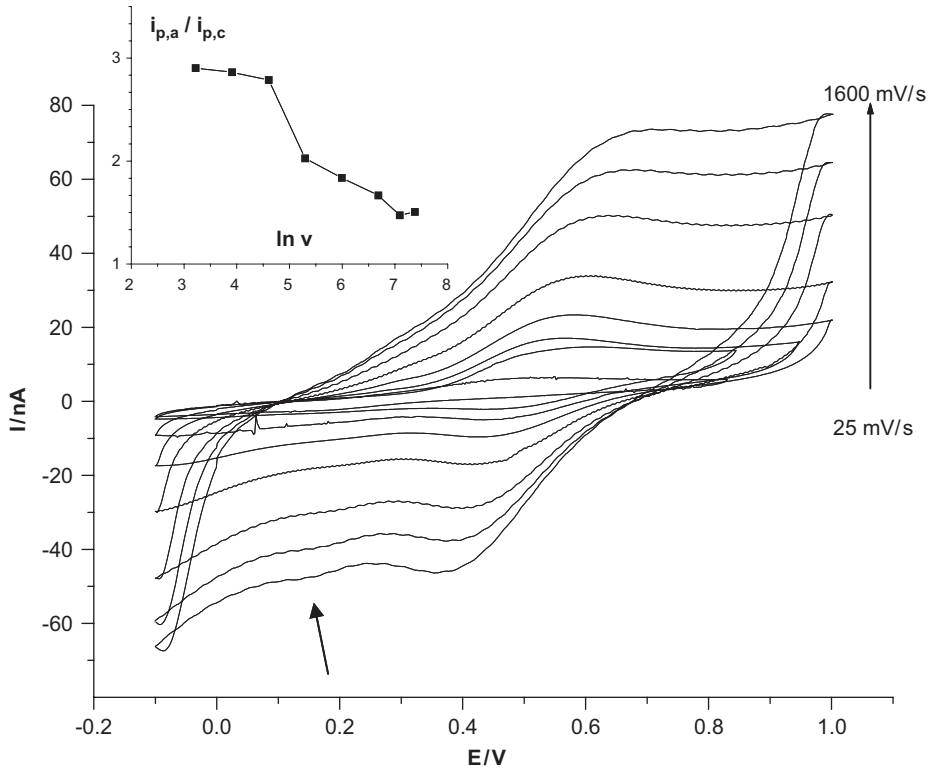


Fig. 4. Cyclic voltammograms of $KDyFe(CN)_6$ with cavity microelectrode in 1.0 M KCl aqueous solution at a scan rate of 25, 50, 100, 200, 400, 800, 1200 and 1600 mV/s. Inset: plot of the ratio of anodic current to cathodic current as function of the logarithm of the scan rate.

Table 1
Electrochemical data recorded during cyclic voltametry experiment performed on the dysprosium hexacyanoferrate compound into the cavity microelectrode

| $V$ (mV s$^{-1}$) | 25 | 50 | 100 | 200 | 400 | 800 | 1200 | 1600 |
|---|---|---|---|---|---|---|---|---|
| $i_{p,a}$ (nA) | 6.3 | 14.6 | 17 | 23.5 | 31.4 | 49.8 | 62 | 74 |
| $E_{p,a}$ (mV) | 533 | 540 | 562 | 578 | 604 | 637 | 677 | 694 |
| $i_{p,c}$ (nA) | −2.8 | −5.1 | −6.1 | −11.6 | −17.1 | −27.9 | −42.1 | −46.1 |
| $E_{p,c}$ (mV) | 470 | 462 | 451 | 436 | 414 | 396 | 385 | 381 |
| $\Delta E_p$ (mV) | 63 | 78 | 111 | 142 | 190 | 241 | 292 | 313 |

corresponds to the loose of one $K^+$:

$$[KDyFe^{II}(CN)_6] \underset{}{\overset{(E),\ E^\circ_1}{\rightleftharpoons}} [KDyFe^{III}(CN)_6]^+ + e^- \quad (3)$$

$$(C) \uparrow\downarrow$$

$$[DyFe^{III}(CN)_6] + K^+$$

A more careful look at the CVs displayed in Fig. 4 reveals the timid presence of a reductive peak at 0.15 V betraying the existence a second redox couple at about $E^\circ_2 = 0.20$ V (see arrow on Fig. 4). In the rare-earth hexacyanoferrate serie, Wu et al. [28] have demonstrate that such behavior was typical of $DyFe(CN)_6$. It was postulated that the size of the particle may be the reason of the existence of two redox peaks. These results were supported by the comparison of $DyFe(CN)_6$ chemically and electrochemically generated and by comparing their size by mean of electronic microscopy. However, the authors do not explain why this behavior is specific to the dysprosium ion. That's the reason we suppose another possibility: the origin of these two redox peaks may be explained by the following hypothetic square-scheme:

$$\begin{array}{ccc} [KDyFe^{II}(CN)_6] & \underset{(E^\circ_1)}{\overset{\mathbf{I}}{\rightleftharpoons}} & [KDyFe^{III}(CN)_6]^+ \\ K^+ \ \mathbf{IV} & & \mathbf{II} \ K^+ \\ [DyFe^{II}(CN)_6]^- & \underset{(E^\circ_2)}{\overset{\mathbf{III}}{\rightleftharpoons}} & [DyFe^{III}(CN)_6] \end{array} \quad (4)$$

The square scheme is supported by the fact that after oxidation, there are two reductive peaks current, so there are two kinds of backward routes leading to the same initial compound. **I** and **III** are two redox processes characterized with $E^\circ_1$ and $E^\circ_2$, respectively, with $E^\circ_1 > E^\circ_2$. $E^\circ_1$ and $E^\circ_2$ are assumed to be different since the iron atom is differently surrounded. **II** and **IV** are the chemical step where $K^+$ is exchanged for charge compensation. Usually, the square-schemes are helpful to explain the shift of a peak potential when a ligand surrounds a redox center. The potential shift is accompanied by a

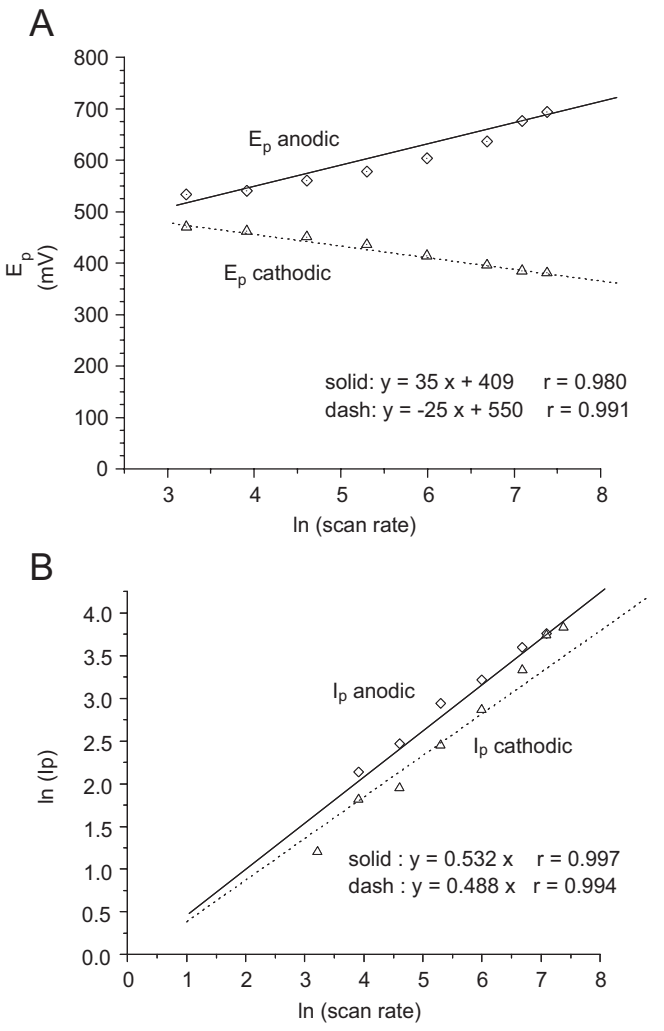


Fig. 5. (A) Variation of the anodic and cathodic peak potential as a function of the logarithm of the scan rate. (B) Variation of the anodic and cathodic peak currents as a function of the scan rate in log plot.

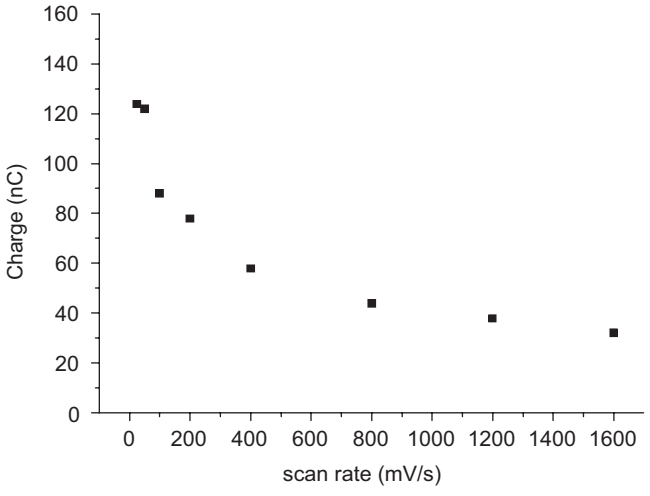


Fig. 6. Variation of the anodic charge from CVs as a function of the scan rate in the same experimental conditions as in Fig. 5.

modification of complex geometry. Here, such behavior is not valid: Xiaoyu et al. [39] have demonstrated that both $KDyFe(CN)_6$ and $DyFe(CN)_6$ crystallize in orthorhombic space group *Cmcm*. During the oxidation of the hexacyanoferrate, the pathway is **I** then **II**, leading to $DyFe(CN)_6$. The backward route is a competition between (**III**, **IV**) and (**−II**, **−I**). Given that $E^\circ_1 > E^\circ_2$, the preferential pathway for the reduction is (**−II**, **−I**). However at high scan rates, the pathway (**III**, **IV**) appears on the cyclic voltamograms with a second peak current at 0.15 V. This point supports the high values of $\Delta E_p$ we obtain for the first redox system ($E^\circ_1$).

The structural study shows the implication on the diffusion of the $K^+$ through preferential directions inside the microcrystalline material. The tunnel structure can accommodate not only neutral water molecules but also charged species balanced by the iron valence state. This behavior is commonly accepted in literature [25–28,40]. $K^+$ ions can move along the conductions channels by hopping between each $K^+$ site, these ions should move through the lateral faces of the polyhedra which hence, operate as bottlenecks. The sides of the lateral faces can be easily calculated from the nitrogen and oxygen coordinates and the lattice parameters of the crystal structure. The radius of the circumscribed circumference was determined. This radius is taken hereafter as a measure of the bottleneck size, insofar as this distance minus oxygen or nitrogen radius of the biggest sphere that can through the bottleneck. The bottleneck size of lateral faces down the equatorial plan equal to 0.216 nm is narrower that of lateral faces up the equatorial plan equal to 0.261 nm indicating a preferentially ionic conduction between this latter faces. The tunnel cross-section is primarily influenced by the size of lanthanide ion. Fig. 2 shows the 3-D framework of $KDyFe(CN)_6 \cdot 3.5H_2O$. Further investigations are necessary to explore the possibility that the dimensionality of the material (i.e. a fractal-like structure) can give new insights on the structure/diffusion properties relationship [41]. Such study remains somewhat complex due to the multipart nature of the $KDyFe(CN)_6$: commonly, the electrochemical probes employed to study the fractal dimension of a material are typically based on ferrocene (or derivatives) redox couple.

## 4. Conclusion

Microcrystalline $KDyFe(CN)_6$ solid was synthesized and the transport properties upon electronic transfer was studied by mean of cavity microelectrode. The electrochemical data got from cyclic voltametry indicate that the charge transfer is followed by $K^+$ cation diffusion inside the microstructure in order to ensure charge compensation. X-ray data tend to indicate that these cations move into preferential direction, i.e. channel-like structures. The structure–transport properties relationship was confirmed by the fact that the transport is limited by the diffusion of $K^+$ inside the solid.

## Acknowledgments

Authors acknowledge Pr Randriamahazaka (ITODYS—Université de Paris VII) and Dr. Yu (UMR 7582 CNRS—Université Paris Val de Marne) and the CME Network (CNRS—France) for supplying the cavity microelectrodes.

## References

[1] A.G. Sharpe, in: The Chemistry of Cyano Complexes of the Transition Metals, Academic Press, New York, 1976.
[2] K. Itaya, I. Uchida, V.D. Neff, Acc. Chem. Res. 19 (1986) 162–168.
[3] V.D. Neff, J. Electrochem. Soc. 125 (1978) 886–887.
[4] D. Ellis, M. Eckhoff, V.D. Neff, J. Phys. Chem. 85 (1981) 1225–1231.
[5] K. Itaya, T. Ataka, S. Toshima, J. Am. Chem. Soc. 104 (1982) 4767–4772.
[6] R.J. Mortimer, D.R. Rosseinsky, J. Electroanal. Chem. 151 (1983) 133–147.
[7] B.J. Feldman, O.R. Melroy, J. Electroanal. Chem. 234 (1987) 213–227.
[8] C.A. Lundgren, R.W. Murray, Inorg. Chem. 27 (1988) 933–939.
[9] D.E. Stilwell, K.H. Park, M.H. Miles, J. Appl. Electrochem. 22 (1992) 325–331.
[10] A. Roig, J. Navarro, J.J. Garcia, F. Vicente, Electrochim. Acta 39 (1994) 437–442.
[11] A. Dostal, B. Meyer, F. Scholz, U. Schröder, A.M. Bond, F. Marken, S.J. Shaw, J. Phys. Chem. 99 (1995) 2096–2103.
[12] L.J. Amos, A. Duggal, E.J. Mirsky, P. Ragonesi, A.B. Bocarsly, P.A. Fitzgerald-Bocarsly, Anal. Chem. 60 (1988) 245–249.
[13] P.M.S. Monk, R.J. Mortiner, D.R. Rosseinsky, in: Electrochromism, Fundamentals and Applications, VCH, Weinheim, 1995 (Chapter 6).
[14] P.J. Kulesza, Inorg. Chem. 29 (1990) 2395–2397.
[15] A. Xidis, V.D. Neff, J. Electrochem. Soc. 138 (1991) 3637–3642.
[16] V.D. Neff, J. Electrochem. Soc. 132 (1985) 1382–1384.
[17] W. Prandtl, S. Mohr, Z. Anorg. Allg. Chem. 236 (1938) 243–251.
[18] G.W. Beall, D.F. Mullica, W.O. Milligan, J. Korp, I. Bernal, Acta Crystallogr. B 34 (1978) 1446–1449.
[19] D.F. Mullica, W.O. Milligan, J.D. Oliver, Inorg. Nucl. Chem. Lett. 15 (1979) 1–5.
[20] D.F. Mullica, E.L. Sappenfield, Powder Diffraction 4 (2) (1989) 101–102.
[21] D.F. Mullica, E.L. Sappenfield, T.A. Curnigham, J. Solid State Chem. 91 (1991) 98–104.
[22] F. Goubard, A. Tabuteau, J. Solid State Chem. 167 (2002) 34–40.
[23] F. Goubard, A. Tabuteau, Struct. Chem. 14 (3) (2003) 257–262.
[24] P. Hulliger, H. Vetsch, X.-L. Xu, J. Alloys Compd. 181 (1992) 489–493.
[25] S.Q. Liu, H.Y. Chen, J. Electroanal. Chem. 528 (2002) 190–195.
[26] P. Wu, C. Cai, J. Solid State Electrochem. 8 (2004) 538–543.
[27] P. Wu, S. Lu, C. Cai, J. Electroanal. Chem. 569 (2004) 143–150.
[28] P. Wu, Y. Shi, C. Cai, J. Solid State Electrochem. 10 (2006) 270–276.
[29] R. Vallot, A. N'Diaye, A. Bermont, C. Jakubowicz, L.T. Yu, Electrochim. Acta 25 (1980) 1501–1512.
[30] J.M. Cocciantelli, P. Gravereau, J.P. Doumerc, M. Pouchard, P. Hagenmuller, J. Solid State Chem. 93 (1991) 497–502.
[31] A. Dostal, U. Scröder, F. Scholz, Inorg. Chem. 34 (1995) 1711–1717.
[32] V. Vivier, C. Cachet-Vivier, B.L. Wu, C.S. Cha, J.Y. Nedelec, L.T. Yu, Electrochem. Solid State Lett. 2 (1999) 385–387.
[33] V. Vivier, C. Cachet-Vivier, C.S. Cha, J.Y. Nedelec, L.T. Yu, Electrochem. Commun. 2 (2000) 180–185.
[34] C. Cachet-Vivier, V. Vivier, C.S. Cha, J.Y. Nedelec, L.T. Yu, Electrochim. Acta 47 (2001) 181–189.
[35] E. Laviron, J. Electroanal. Chem. 112 (1980) 1–9.
[36] E. Laviron, L. Roullier, C. Degrand, J. Electroanal. Chem. 112 (1980) 11–23.
[37] E. Laviron, J. Electroanal. Chem. 122 (1981) 37–44.
[38] A.J. Bard, L.R. Faulkner, Electrochemical Methods, Wiley, New York, 1980.
[39] W. Xiaoyu, Y. Yukawa, Y. Masuda, J. Alloys Compd. 290 (1999) 85–90.
[40] A.J. Kuzela, M.A. Malik, M. Berrettoni, M. Giorgetti, S. Zamponi, R. Schmidt, R. Marassi, J. Phys. Chem. B 102 (1998) 1870–1879.
[41] C.P. Andrieux, P. Audebert, J. Phys. Chem. B 105 (2001) 444–448.